optica

Background-free broadband absorption spectroscopy based on interferometric suppression with a sign-inverted waveform

Teemu Tomberg,[1] Andrey Muraviev,[2] Qitian Ru,[2] and Konstantin L. Vodopyanov[2,*]

[1]Department of Chemistry, University of Helsinki, Helsinki 00560, Finland
[2]CREOL, College of Optics and Photonics, University of Central Florida, Orlando, Florida 32816, USA
*Corresponding author: vodopyanov@creol.ucf.edu

Received 20 August 2018; revised 28 November 2018; accepted 17 December 2018 (Doc. ID 342639); published 28 January 2019

Background-free methods have potentially superior detection sensitivity because of their ability to take advantage of the full laser power; they are therefore attractive to spectroscopists. We implement background-free Fourier transform spectroscopy based on coherent suppression of the background using an interferometer, whereby the central peak of the interferogram is suppressed without losing molecular absorption signatures. This results in the appearance of peaks rather than dips in the measured spectrum. The technique can be used with a variety of broadband spectroscopies and features advantages such as a reduction in the required detector dynamic range, the capability to perform quantitative measurements, and strongly enhanced sensitivity down to the quantum limit. We validated our method experimentally by performing mid-infrared dual-comb spectroscopy with a mixture of multiple molecular species over a broad wavelength range of 3–5 μm.

https://doi.org/10.1364/OPTICA.6.000147

1. INTRODUCTION

Absorption spectroscopy is a powerful tool for detecting trace amounts of atoms, molecules, and ions. It relies upon light attenuation caused by resonant absorption. Detecting trace amounts of absorbents, such as gaseous molecules with low, part per billion (ppb) to part per trillion (ppt), concentrations imposes strict requirements on the stability of the laser output since shallow absorption dips in the spectrum may not be seen due to laser spectral density fluctuations.

Background-free spectroscopy methods are most attractive for ultrasensitive detection, because requirements for the laser stability are considerably relaxed. The existing background-free (BF) laser spectroscopic techniques include photoacoustic spectroscopy [1,2], Faraday rotation spectroscopy [3,4], and laser-induced fluorescence spectroscopy [5,6]. However, they have their own drawbacks. For example, photoacoustic spectroscopy cannot be used at low gas pressures and the access to narrow (e.g., Doppler-broadened) resonances is limited; in addition, the photoacoustic efficiency strongly varies between different molecules, which makes quantitative measurements difficult. On the other hand, Faraday rotation spectroscopy is applicable only to a small class of molecules, radicals such as the NO molecule, and laser-induced fluorescence spectroscopy is mostly limited to the visible and UV ranges.

In this paper, we propose a BF method in which the background that does not carry spectroscopic information is eliminated through interferometric suppression with a sign-inverted waveform. The most salient features of our method are applicability to any absorbing media, exceedingly relaxed constraints for the dynamic range of an optical detector plus data acquisition system, capability for quantitative analysis, and superior sensitivity that can reach the quantum limit.

To a great extent, the inspiration for our method came from advanced laser-based gravitational wave detectors that use a Michelson-type interferometer operating close to a dark fringe, such that transmission of the "carrier" laser light to the output port is strongly suppressed [7]. Also, our method bears resemblance to the dual-beam interferometry, in which the lower spatial frequencies of a background field are interferometrically suppressed, thereby enhancing the detectability of localized sources [8], and is similar to prior demonstrations of single-frequency quasi-zero-background tunable laser absorption spectroscopy performed in a narrow range of frequencies [9,10]. Likewise, we were motivated by the work of Ref. [11], where the authors proposed frequency-comb spectroscopic measurements based on an interferometer, with suppression of the background by adjusting the path difference between the interferometer arms. However, tuning the path difference can adjust the relative phase only locally in the frequency space, and no procedure was described on how to preserve the relative phase of π radians over a large span of frequencies. Several papers were published on noise reduction in Fourier transform spectroscopy (FTS) using electronic differential processing of the signals from separate balanced photodetectors, or phase-sensitive

detection on a single detector (see [12] and references therein). We emphasize that the main feature of our method is coherent adding optical fields rather than signals from square-law detectors.

The advantages of our BF technique become especially noticeable when applied to broadband dual-comb spectroscopy—a time-coherent version of FTS [13]. Combining two phase-locked frequency combs into a spectrometer allows fast and broadband measurements, clearly surpassing conventional FTS in speed, spectral resolution, and absolute frequency accuracy [14,15]. Yet, the sensitivity of a broadband dual-comb spectrometer is limited by fluctuations of the optical spectral density and, for example, absorption spectroscopy with tunable lasers can reach higher sensitivity, although at the expense of smaller spectral coverage [16]. In dual-comb spectroscopy, the signal is in the form of periodic interferograms with a period of $1/\Delta f_{\text{rep}}$ (ms to μs range), where Δf_{rep} is an offset of repetition frequencies (f_{rep}) between the two combs. Molecular absorption features reveal themselves as a free-induction decay in the form of periodic oscillations that originate from the rephasing of the multiply excited rovibrational states. The information on the molecular absorption resides in the low-amplitude tails of the interferogram, with the amplitude being orders of magnitude smaller than that of the central peak. This imposes severe constraints on the dynamic range of both a photodetector and a data acquisition system.

2. APPROACH

The essence of our approach is to eliminate the central peak of the interferogram by coherently combining the optical waveform with its sign-inverted replica that was not affected by the absorbent. This can be done by several methods, including the use of a broadband dark-fringe Michelson interferometer, as illustrated in Fig. 1. The design of Fig. 1(a) uses a symmetric beamsplitter (BS) made of a thin ($<\lambda$) dielectric, e.g., a pellicle, so that both surfaces contribute to the reflection. A reflective 1:1 telescope in one of the arms flips the phase by π radians due to the Gouy phase shift. The design of Fig. 1(b) uses a thick dielectric plate (ideally with a high refractive index) as a beamsplitter; the asymmetry arises from the fact that the internal and external reflections from the BS interface differ in phase by π [17]. (A compensating plate of the same thickness needs to be added to one of the arms to equalize group dispersion between the two arms.) In both cases, an absorbing "sample" cell is placed in arm 1 of the interferometer and an

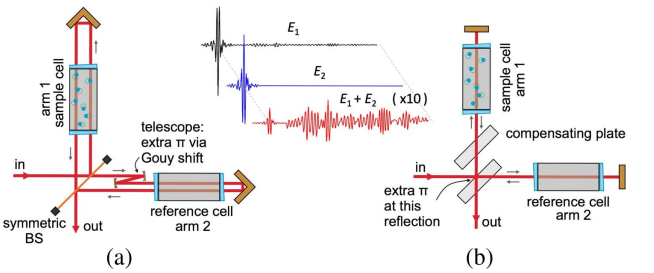

Fig. 1. Two examples for BF spectroscopic detection using a dark-fringe Michelson-type interferometer with (a) a symmetric beam splitter (BS) and (b) a telescope in one arm that flips the phase by π radians. In (b), an asymmetric BS (a dielectric plate) is used, whereby the external and internal reflections have the relative phase shift of π. The inset (based on our real interferograms) is the electric-field representation of the dark-fringe interference.

identical "reference" cell is placed in arm 2. Such an optical system works as a balanced detector: any extra absorption in the "sample" cell results in the appearance of a signal. For the broadband performance, all parameters such as group delay, group delay dispersion, and optical field amplitudes in both arms need to be balanced. This imposes strict constraints on the tolerance with respect to the thickness of the optical elements (down to a few μm).

In a transmission experiment, the intensity transmission function at a given optical frequency is $T(\nu) = e^{-A(\nu)}$, where $A(\nu)$ is the intensity profile of the spectral line (absorbance) with the peak value A_0. For $A_0 \ll 1$, the fractional decrease of the spectral power at the line center is A_0. If the optical power at the detector is high enough, so that the laser noise dominates, the signal-to-noise ratio (SNR) is A_0/σ, where σ is a relative standard deviation of the optical power spectral density. In our BF measurement, the two interfering waveforms are balanced in amplitude and have opposite signs. In addition, the first beam passes through an absorber. For $A_0 \ll 1$, the electric fields for the two beams at the absorption line center are

$$E_1 = -E_0(1 - \delta - A_0/2) \quad \text{and} \quad E_2 = E_0. \tag{1}$$

Here, $\delta \ll 1$ is an E-field unbalance factor (assume δ is real for now), and $P_0 \sim E_0^2$ is the associated comb-mode power. The total field is

$$E(\nu) = E_1 + E_2 = E_0(\delta + A_0/2), \tag{2}$$

and the comb-mode power reaching a photodetector is

$$P_{\text{det}} \sim E^2 \sim P_0(\delta^2 + A_0\delta + A_0^2/4). \tag{3}$$

For the most interesting case of detecting weak absorption features, $A \ll \delta$, the last term can be neglected. In this case, the dominating first term ($P_0\delta^2$) plays the role of a local oscillator and represents a fluctuating background, while the second term is the BF signal that mimics the absorbance spectrum $A(\nu)$. The signal-to-noise ratio is then

$$\text{SNR} = \frac{P_0 A_0 \delta}{\sqrt{(P_{N,\text{las}})^2 + (P_{N,\text{shot}})^2 + (P_{N,\text{det}})^2}}, \tag{4}$$

where $P_{N,\text{las}} = \sigma(P_0\delta^2)$ is associated with the laser noise, $P_{N,\text{shot}}$ is the quantum (shot) noise of the laser power at the detector, and $P_{N,\text{det}}$ is the photodetector noise equivalent power. (We estimated that in our experiment, the detector noise becomes dominant when the total optical power at the detector is less than 0.3 mW.) When the laser noise dominates, SNR $= (1/\delta)(A_0/\sigma)$. Hence, with reduction of the unbalance factor, SNR increases as $1/\delta$. However, this comes at the expense of reducing (as δ^2) the optical power reaching the detector. Even if we neglect the detector noise, at some point the shot noise $P_{N,\text{shot}} = \sqrt{(P_0\delta^2)(h\nu)\Delta f}$ will dominate, and SNR will no longer improve with reducing δ (here, $h\nu$ is the photon energy and Δf is the detection bandwidth; we also assumed unit quantum efficiency). To ensure that SNR still increases with reducing δ, one needs to scale up the laser power, which translates into $P_{N,\text{las}} > P_{N,\text{shot}}$ or $P_0 > h\nu\Delta f/(\sigma\delta)^2$. In fact, at a given laser power, the unbalance factor δ can be optimized for the best performance [9]. This is analogous to offsetting from the interferometer dark fringe that is used to improve the sensitivity of advanced gravitational wave detectors [7]. Since in frequency comb spectroscopy the spectrum is sampled by comb modes, our estimate for P_0 refers to the power per comb mode.

In our case, we have some 260,000 comb lines at the –3 dB level; hence, the total comb power needs to be $P_{\text{total}} > 0.8$ mW for $\delta = 0.1$, >78 mW for $\delta = 0.01$, and as high as 7.8 W for $\delta = 0.001$. We assume that in our dual-comb experiment the comb is centered near $\lambda \approx 4$ μm, $\sigma = 0.3$ for a single interferogram with no averaging, and $\Delta f = 60$ MHz.

3. EXPERIMENT

For testing our method, we used a mid-IR dual-comb system described in detail in [15]. Briefly, the system (Fig. 2) consisted of two identical and phase-locked GaAs subharmonic optical parametric oscillators (OPOs) pumped in turn by two optically referenced, phase-locked thulium-fiber laser frequency combs. The main parameters of the dual-comb system were instantaneous spectral span 3.14–5.45 μm (at –25 dB), repetition rate $f_{\text{rep}} = 115$ MHz, $\Delta f_{\text{rep}} = 138.5$ Hz, and spectral resolution 0.0038 cm^{-1}. The outputs of the two OPOs were combined on a pellicle Thorlabs BP145B4 beamsplitter (BS1 in Fig. 2) such that one of the outputs was used to trigger the data-acquisition system, while the other (with 7 mW of the combined average power) was directed to the BF interferometer. For detecting dual-comb interferograms, we used a fast (60 MHz) cooled (77 K) InSb detector. The optical spectra were retrieved from the interferograms via fast Fourier transform [15].

The Michelson interferometer for our BF spectroscopy utilized a 50:50 Thorlabs BSW511 beamsplitter (BS2 in Fig. 2) on a wedged (0.5-deg) 5-mm-thick CaF_2 substrate (flatness $\lambda/8$ at 633 nm), with dielectric coating on the front surface designed for the 1–6 μm range. Ideally, the beamsplitter would be an uncoated dielectric plate which gives the desired phase difference of π. However, since the Fresnel reflection of CaF_2 is low, for this pilot demonstration we used a coated BS with unspecified phase relation between internal and external reflections. We used the same type CaF_2 wedged substrates as windows in our 80-mm-long sample and reference gas cells (Fig. 2). One of the two gold-coated interferometer end mirrors (flatness $\lambda/10$) was mounted on a motorized translation stage for adjusting the optical path difference (OPD) to zero, whereas piezo actuators (PZT) were used on both mirrors for fine-tuning and active stabilization of the OPD against thermal fluctuations, to achieve the interferometer dark-fringe output. We used the "dither-and-lock" method for OPD stabilization, with a servo loop time constant of ~1 s. The best background suppression achieved in the dark-fringe mode was 250, that is, the peak-to-peak amplitude of the interferogram was 0.4% of the one when the second arm was blocked.

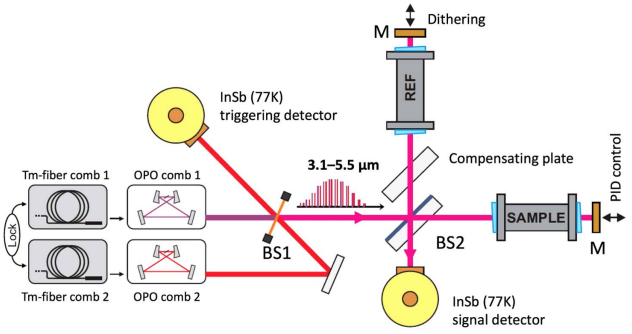

Fig. 2. Schematic of the mid-IR dual-comb system together with the Michelson interferometer assembled for background-free spectroscopy. M, gold-coated mirrors; BS1 and BS2, beam splitters.

4. RESULTS AND DISCUSSION

Figure 3 displays the results of the dual-comb spectral measurements performed over the whole 3–5-μm "instantaneous" spectrum. The "sample" cell was filled with a mixture of five molecular gases with the following volume mixing ratios: CO (0.25%), C_2H_6 (0.20%), C_2H_4 (0.35%), CH_4 (0.22%), and N_2O (0.12%) in an N_2 buffer gas at 120 mbar total pressure, while the "reference" cell was evacuated. One measurement [Fig. 3(a)] was taken in the transmission mode (T-mode), while the other [Fig. 3(b)] was taken in the background-free mode (BF-mode). Both plots correspond to ~20,000 coherently averaged dual-comb interferograms (measurement time 145 s). In the T-mode, the spectrum was taken by blocking the interferometer "reference" arm. In order to avoid detector saturation, the total optical power reaching the detector was reduced to 150 μW by 1:10 beam attenuation. In the BF-mode, the power at the detector (suppressed due to the dark-fringe interference) was ~50 μW, and no beam attenuation was used. This power was a few times below the optimal for detector performance. One can see from Figs. 3(c) and 3(d) that there is a good correlation between absorption peaks pointing down (T-mode) and up (BF-mode), except for the region 2300–2400 cm^{-1} associated with strong CO_2 absorption in room air.

Due to their interferometric nature, our BF measurements are phase-sensitive. To simulate BF lineshapes, we used the complex representation of absorption spectral lines, to include dispersion of the refractive index. The latter is connected to the intensity absorption spectrum via the Kramers–Kronig relations and can be retrieved numerically from a known absorption spectrum. For $p \sim 100$ mbar gas pressure used in our experiment, we were able to use a simple Lorentzian line profile and write a complex transmission function for the optical E-field in the form $t(\nu) = \exp(-\frac{A_0/2}{1+i(\nu-\nu_0)/\gamma})$, where $A_0/2$ is the *amplitude* loss at the center frequency ν_0, and γ is the line half-width. The unbalance factor δ should also be written in the complex form $\delta(\nu)e^{i\varphi(\nu)}$, to take into account the fact that the relative phase between the two arms can deviate from π in some spectral regions. Thus, the laser power at a given comb mode seen by a detector is

$$P = (E_1 + E_2)^2 = P_0|1 - (1 - \delta e^{i\varphi})t|^2, \tag{5}$$

where P_0 corresponds to the case when the "signal" arm is blocked. A normalized BF spectrum then takes a general form:

$$S(\nu) = |1 - [1 - \delta(\nu)e^{i\varphi(\nu)}]t(\nu)|^2. \tag{6}$$

Figures 3(e)–3(h) shows absorbance $A(\nu)$ spectra (inverted for clarity) derived from T-mode in a standard fashion and normalized BF spectra $S(\nu)$ (pointing up) derived from BF-mode, for the selected absorption peaks of CO, N_2O, and C_2H_6 molecules [marked as "A"–"D" in Figs. 3(c) and 3(d)]. The lineshapes for both $A(\nu)$ and $S(\nu)$ are in good agreement with theory in terms of line center, linewidth, and lineshape: in the case of T-mode with HITRAN database simulations [18], and for BF-mode with simulations based on Eq. (6), HITRAN database, and best-fitted $\delta(\nu)$ and $\varphi(\nu)$ that are shown in Figs. 3(i) and 3(j). Equation (6) also well accounts for the asymmetric (dispersive) $S(\nu)$ lineshapes of Figs. 3(g) and 3(h), corresponding to some dephasing between the

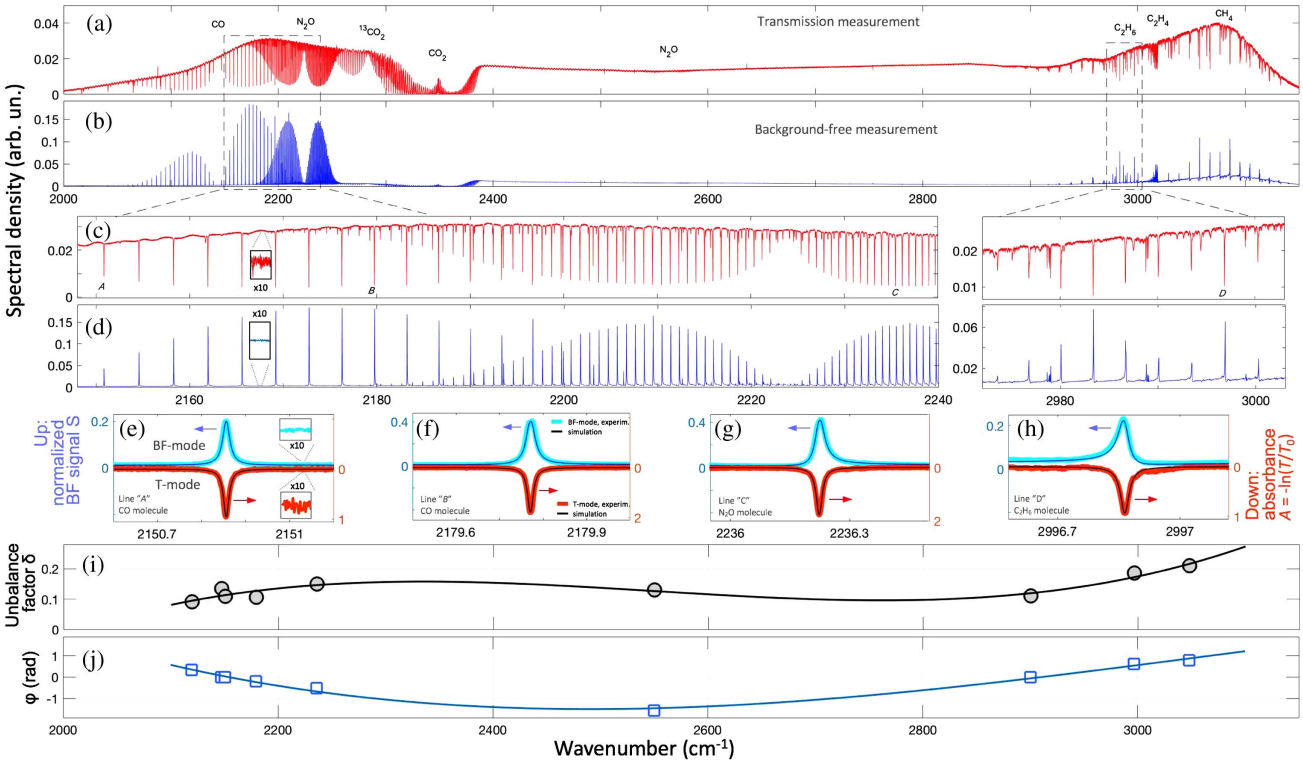

Fig. 3. Raw dual-comb spectra measured in (a) T-mode and (b) BF-mode. Horizontally zoomed spectra for (c) T-mode and (d) BF-mode. (e)–(h) Pointing down: absorbance $A(\nu)$ spectra derived from T-mode. Pointing up: normalized BF spectra derived from BF-mode for absorption peaks of CO, N_2O, and C_2H_6 molecules. Thick lines, experimental; thin lines, simulation. The insets show vertically zoomed background. (i) and (j) Best fitted values for the unbalance factor δ and its phase angle ϕ; both are fitted in turn by cubic polynomials (solid lines).

arms ($\varphi \neq 0$) possibly caused by dispersion in the beamsplitter or unbalanced thicknesses of the optical elements.

We note that our BF method is quantitative in the sense that, by fitting $S(\nu)$ spectra using spectral libraries and known $\delta(\nu)$ and $\varphi(\nu)$ (both are the property of the interferometer itself), one can extract absolute absorbances and, hence, absolute analyte concentrations.

Despite the limited optical power (at the time of the experiment, the dual-comb system was configured for a low-power output), we observed a considerable 3–10 times SNR improvement with the BF technique. The insets to Figs. 3(c)–3(e) give the idea of noise reduction by showing vertically zoomed background spectra. For example, for detection of CO rovibrational peaks near 2170 cm^{-1} [Figs. 3(c) and 3(d)], SNR in the raw spectra was 107.6 $Hz^{1/2}$ (BF-mode) versus 12.8 $Hz^{1/2}$ (T-mode), that is, we observed 8.4 times SNR improvement. Interestingly, parasitic Fabry–Pérot oscillations seen in the T-mode [Fig. 3(c)] are not present in the BF-mode [Fig. 3(d)].

5. CONCLUSION

We present and experimentally validate a new method for background-free and quantitative spectroscopy based on interferometric suppression with a sign-inverted waveform, a promise of significantly enhanced detection sensitivity, and reduced requirements for the detector dynamic range. In this pilot demonstration, we have demonstrated a noticeable SNR improvement over the transmission-mode measurements, despite the fact that the quality of the off-the-shelf optics prevented us from achieving a uniform (over frequency) dark-fringe contrast, and also despite the limited optical power. Watt-level broadband mid-IR frequency combs reported recently by several groups [19–21] would be beneficial to achieving quantum-limited detection in future. Finally, we consider our background-free method to be applicable to a variety of broadband spectroscopic techniques: from traditional FTS using incoherent sources, FTS using frequency combs, frequency-comb spectroscopy with virtually imaged phase arrays, and coherent dual-comb spectroscopy to tunable-laser spectroscopy and time-domain spectroscopy with electro-optic sampling.

Funding. Office of Naval Research (ONR) (N00014-15-1-2659); Defense Advanced Research Projects Agency (DARPA) (W31P4Q-15-1-0008); Jenny ja Antti Wihurin Rahasto; CHEMS doctoral program, Helsingin Yliopisto.

Acknowledgment. We thank Miao Zhu and Boris Zeldovich for stimulating discussions.

REFERENCES

1. A. A. Kosterev, Y. A. Bakhirkin, R. F. Curl, and F. K. Tittel, "Quartz-enhanced photoacoustic spectroscopy," Opt. Lett. **27**, 1902–1904 (2002).
2. V. Koskinen, J. Fonsen, J. Kauppinen, and I. Kauppinen, "Extremely sensitive trace gas analysis with modern photoacoustic spectroscopy," Vib. Spectrosc. **42**, 239–242 (2006).
3. G. Litfin, C. R. Pollock, R. F. Curl, and F. K. Tittel, "Sensitivity enhancement of laser absorption spectroscopy by magnetic rotation effect," J. Chem. Phys. **72**, 6602–6605 (1980).

4. H. Ganser, M. Horstjann, C. V. Suschek, P. Hering, and M. Mürtz, "Online monitoring of biogenic nitric oxide with a QC laser-based Faraday modulation technique," Appl. Phys. B **78**, 513–517 (2004).
5. W. M. Fairbank, T. W. Hänsen, and A. L. Schawlow, "Absolute measurement of very low sodium-vapor densities using laser resonance fluorescence," J. Opt. Soc. Am. **65**, 199–204 (1975).
6. W. Neuhauser, M. Hohenstatt, P. E. Toschek, and H. Dehmelt, "Localized visible Ba^+ mono-ion oscillator," Phys. Rev. A **22**, 1137–1140 (1980).
7. T. T. Fricke, N. D. Smith-Lefebvre, R. Abbott, R. Adhikari, K. L. Dooley, M. Evans, P. Fritschel, V. V. Frolov, K. Kawabe, J. S. Kissel, B. J. J. Slagmolen, and S. J. Waldman, "DC readout experiment in enhanced LIGO," Classical Quantum Gravity **29**, 065005 (2012).
8. T. F. Zehnpfennig, O. Shepherd, S. Rappaport, W. P. Reidy, and G. Vanasse, "Background suppression in double-beam interferometry," Appl. Opt. **18**, 1996–2002 (1979).
9. Z. Guan, M. Lewander, and S. Svanberg, "Quasi zero-background tunable diode laser absorption spectroscopy employing a balanced Michelson interferometer," Opt. Express **16**, 21714–21720 (2008).
10. J. Hayden, S. Hugger, F. Fuchs, and B. Lendl, "A quantum cascade laser-based Mach–Zehnder interferometer for chemical sensing employing molecular absorption and dispersion," Appl. Phys. B **124**, 29 (2018).
11. M. Zhu, A. Kleczewski, and R. C. Taber, "System for performing optical spectroscopy including interferometer," U.S. patent 9, 341, 516 (May 17, 2016).
12. V. V. Goncharov and G. E. Hall, "Supercontinuum Fourier transform spectrometry with balanced detection on a single photodiode," J. Chem. Phys. **145**, 084201 (2016).
13. I. Coddington, N. Newbury, and W. Swann, "Dual-comb spectroscopy," Optica **3**, 414–426 (2016).
14. G. Ycas, F. R. Giorgetta, E. Baumann, I. Coddington, D. Herman, S. A. Diddams, and N. R. Newbury, "High-coherence mid-infrared dual-comb spectroscopy spanning 2.6 to 5.2 μm," Nat. Photonics **12**, 202–208 (2018).
15. A. V. Muraviev, V. O. Smolski, Z. E. Loparo, and K. L. Vodopyanov, "Massively parallel sensing of trace molecules and their isotopologues with broadband subharmonic mid-infrared frequency combs," Nat. Photonics **12**, 209–214 (2018).
16. D. Nelson, J. Shorter, J. McManus, and M. Zahniser, "Sub-part-per-billion detection of nitric oxide in air using a thermoelectrically cooled mid-infrared quantum cascade laser spectrometer," Appl. Phys. B **75**, 343–350 (2002).
17. M. Born and E. Wolf, *Principles of Optics* (Cambridge University, 1997), pp. 59–64.
18. I. E. Gordon, L. S. Rothman, C. Hill, R. V. Kochanov, Y. Tan, P. F. Bernath, M. Birk, V. Boudon, A. Campargue, K. Chance, B. J. Drouin, J. M. Flaud, R. R. Gamache, J. T. Hodges, D. Jacquemart, V. I. Perevalovm, A. Perrin, K. P. Shine, M. H. Smith, J. Tennyson, G. C. Toon, H. Tran, V. G. Tyuterev, A. Barbé, A. G. Császár, V. M. Devi, T. Furtenbacher, J. J. Harrison, J.-M. Hartmann, A. Jolly, T. J. Johnson, T. Karman, I. Kleiner, A. Kyuberis, J. Loos, O. M. Lyulinm, S. T. Massie, S. N. Mikhailenkom, N. Moazzen-Ahmadi, H. S. P. Müller, O. V. Naumenkom, A. V. Nikitinm, O. L. Polyansky, M. Rey, M. Rotger, S. W. Sharpe, K. Sung, E. Starikovam, S. A. Tashkunm, J. Vander Auwera, G. Wagner, J. Wilzewski, P. Wcis, S. Yu, and E. J. Zak, "The HITRAN 2016 molecular spectroscopic database," J. Quant. Spectrosc. Radiat. Transfer **203**, 3–69 (2017).
19. F. C. Cruz, D. L. Maser, T. Johnson, G. Ycas, A. Klose, F. R. Giorgetta, I. Coddington, and S. A. Diddams, "Midinfrared optical frequency combs based on difference frequency generation for molecular spectroscopy," Opt. Express **23**, 26814–26824 (2015).
20. V. Smolski, S. Vasilyev, I. Moskalev, M. Mirov, Q. Ru, A. Muraviev, P. Schunemann, S. Mirov, V. Gapontsev, and K. Vodopyanov, "Half-watt average power femtosecond source spanning 3-8 μm based on subharmonic generation in GaAs," Appl. Phys. B **124**, 101 (2018).
21. M. Seidel, X. Xiao, S. A. Hussain, G. Arisholm, A. Hartung, K. T. Zawilski, P. G. Schunemann, F. Habel, M. Trubetskov, V. Pervak, O. Pronin, and F. Krausz, "Multi-watt, multi-octave, mid-infrared femtosecond source," Sci. Adv. **4**, eaaq1526 (2018).